Direct Evidence for Negative Grain Boundary Potential in Ca-Doped and Undoped $YBa_2Cu_3O_{7-x}$

Marvin A. Schofield,[1,*] Marco Beleggia,[1] Yimei Zhu,[1] Karsten Guth,[2] and Christian Jooss[2]
[1]*Brookhaven National Laboratory, Upton, New York 11973, USA*
[2]*University of Göttingen, Windausweg 2, 37073 Göttingen, Germany*
(Received 12 September 2003; published 13 May 2004)

Using electron holography in a transmission electron microscope, we obtained direct evidence for the reduction of negative charge at grain boundary dislocations in Ca-doped $YBa_2Cu_3O_7$ (YBCO) when compared to undoped YBCO. Because of the finite width of the valence band in the superconducting CuO_2 planes, the negative grain boundary charge can lead to a depletion of electron holes available for superconductivity. A significant reduction in the size of the perturbed region in the Ca-doped samples appears to be the principal mechanism for the improved interfacial superconductivity.

DOI: 10.1103/PhysRevLett.92.195502 PACS numbers: 61.72.Mm, 61.14.Nm, 73.40.–c, 74.72.Bk

A notion gaining acceptance in recent years is that the electronic properties of highly correlated electrons in transition metal oxides, such as the high-T_c cuprates, are governed by competition between a variety of electronic ground states exhibiting unusual charge, spin, and lattice order [1,2]. Recent experimental work suggests that underdoped, and to some extent optimally doped, high-T_c cuprates are intrinsically inhomogeneous, exhibiting nanoscale electronic phase separation [3,4] where the itinerant holes experience strong electrostatic potential variations [5,6]. The balance between competing ground states is often subtle, and small changes of material parameters (e.g., composition or strain) or the presence of structural disorder can lead to dramatic changes in electronic properties [1,3,4]. The closely related matter of grain boundaries (GB) in high-T_c cuprates accentuates this view, where a proper GB description must account for an experimentally observed insulating layer [7] and measured hole depletion [8,9]. According to the conventional (phenomenological) picture [7,10] developed to understand the improved GB critical current densities in Ca-doped $YBa_2Cu_3O_{7-x}$ (YBCO), a positive interface charge intrinsic to the GB leads to band bending and related depletion of holes. Consequently, there is an insulating state at the GB, and the superconducting order parameter is suppressed. Furthermore, it is speculated, by preferential replacement of Y^{3+} by Ca^{2+}, the positive GB potential is reduced in height, and also in width since Ca doping increases the hole concentration, thereby reducing the electrostatic screening length. Despite, however, the mounting evidence of interface charging playing a significant role in the depression of GB critical current density, there has been no direct observation of the electrostatic potential and charge distribution.

With this in mind, we made a comparison study of 20% Ca-doped and Ca-free $YBa_2Cu_3O_{7-x}$ thin films grown by laser ablation on $SrTiO_3$ bicrystal substrates with pure 4° [001] tilt boundaries. Compared to large-angle grain boundaries, small-angle GBs offer the unique opportunity to reveal the electrostatic properties of separated interfacial dislocation cores, of great advantage for space-charge measurement when probed edge on. Electron holography was primarily used in this study since it allows quantitative measurement of the projected electrostatic potential by reconstructing the phase shift of the electrons passing through the sample [11]. Unlike nanoprobe electron spectroscopy, parallel illumination is used and beam-induced damage is negligible. The superconducting properties of the bicrystal films used in this study were first analyzed at 4.2 K using a magneto-optical (MO) imaging system based on the principle of Faraday rotation [12] to locally measure intra- and intergranular transport properties in a nondissipative, persistent current state of the bicrystals [13]. By comparison of Ca-doped and Ca-free samples we found an increase in J_c of 35% for the 4° [001] tilt boundaries, confirming the improved transport properties by Ca doping for the bicrystals used in this study [14].

Figure 1(a) shows a high-resolution image of the *same* 4° [001] tilt boundary examined by MO experiments and also shows the undisturbed crystal lattice between the ~5.3 nm periodically disordered interfacial dislocation cores. Detailed electron holography experiments were carried out under identical imaging conditions for both doped and undoped YBCO bicrystals under optimized settings to maximize phase sensitivity [15]. The bulk contribution to the measured phase was subtracted to give maps representing contributions due solely to the GB dislocation cores [15], shown in Figs. 1(b)–1(d). The sign of the potential was established during the phase reconstruction of the holograms. The sideband towards the reference wave in vacuum was used, which gave a smaller phase shift at the cores than in the bulk. This corresponds to a negative potential (i.e., closer to the vacuum level) relative to the grain interiors. Since in both doped and undoped cases the GB core potential appears approximately radially symmetric, we extract the measured potential as a function of distance only,

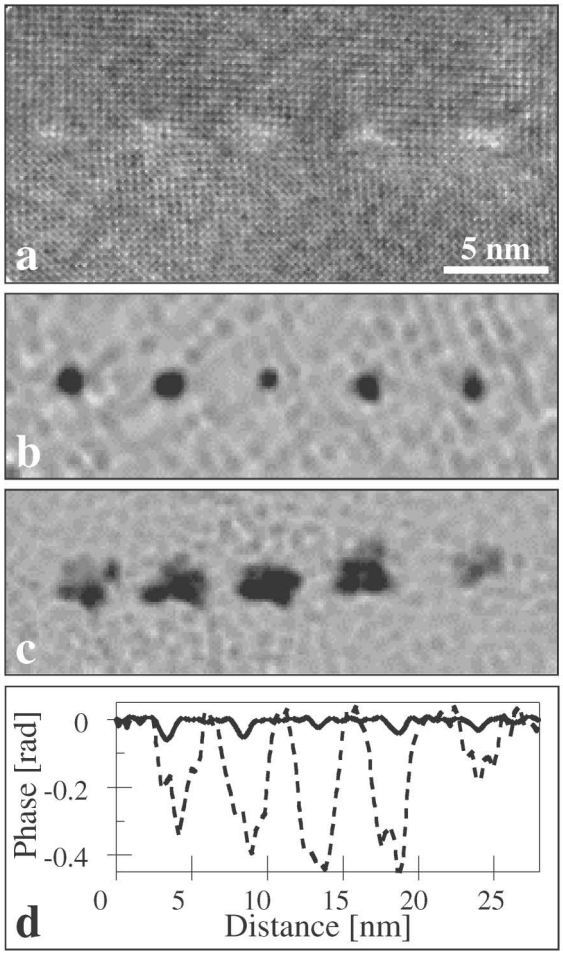

FIG. 1. High-resolution TEM image and reconstructed electron phase. (a) High-resolution image of the 4° [001] tilt boundary in Ca-doped YBCO thin film viewed along the [001] direction. Periodic undisturbed and disturbed regions (dislocation cores) along the boundary are clearly visible. Holograms were recorded with 50 V biprism bias, $37 \times 37\ \mathrm{nm}^2$ field of view, 650 k× magnification, and 2.8 Å interference fringes. Reconstructed phase image, $\phi_{GB}(r)$, showing portions of the GB in the Ca-doped (b) and undoped (c) YBCO and corresponding phase line profiles [(d) solid line, doped; dashed line, undoped]. The difference in thickness between the two samples gives rise to different signal-to-noise ratios visible by comparing (b) and (c). Note in (d) the variation in the phase drop at various core positions due to systematic error associated with removal of the bulk contribution to the measured phase. We correct this effect on physical grounds by assuming that the phase shift is the same for each core position, but at the cost of increased uncertainty in the extracted potential profiles. The projected GB potential, $V_{GB}(r)$, is given by $\phi_{GB}(r) = C_E t V_{GB}(r)$, where $C_E = 6.25 \times 10^{-3}\ \mathrm{V}^{-1}\,\mathrm{nm}^{-1}$ for 300 kV electrons and t is the sample thickness, which was measured from energy filtered images to be 40 and 25 nm for the Ca-free and Ca-doped samples, respectively.

and combine profiles from a number of dislocation cores from each sample as shown in Fig. 2. To facilitate interpretation and quantitative analysis, we fit our data to a Gaussian function (solid line in Fig. 2), which,

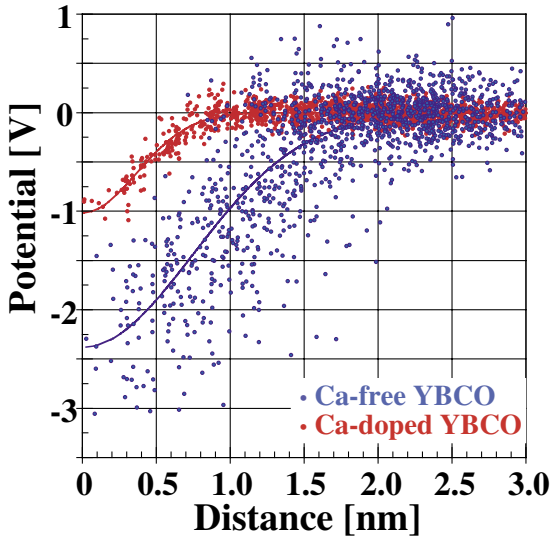

FIG. 2 (color). Measured potential distribution. Distribution of electrostatic potential values as a function of distance from the center of the dislocation cores of the 4° [001] tilt boundary in Ca-doped (red) and undoped (blue) YBCO. Each data set (doped and undoped) represents potential values extracted from five cores. The solid lines are the fitting results of a Gaussian potential distribution. The results (in volts) are measured potentials of $V(r) = -2.4\exp[-r^2/(1.1)^2]$ for Ca-free and $V(r) = -1.0\exp[-r^2/(0.52)^2]$ for Ca-doped YBCO, where r is the radial distance from the core center in nm.

given the spread of the data, we take as experimentally determined.

These measurements give clear and direct evidence that Ca doping in YBCO acts to diminish both the potential drop (from $V_{GB} = 2.4 \pm 0.3$ V to $V_{GB} = 1.0 \pm 0.1$ V) and the spatial extent (from $D = 1.7 \pm 0.3$ nm to $D = 0.8 \pm 0.2$ nm) of the dislocation core potential. In quantifying the GB potential as described above, we measure the potential at the GB relative to the grain interior. Consequently, the measured potential depends on local effects such as changes in stoichiometry, material density, bonding (coordination, length, angles, etc.), lattice strain, structural disorder, etc. While we should expect each of these effects to possibly contribute to the measured potential, a simple description of one predominant cause is difficult since the individual effects are interrelated. Nevertheless, these effects strongly manifest changes in the atomic scattering factors in the forward direction, which directly reflect the local atomic valence. Indeed, our measurements reflect these changes where the valence imbalance between the GB and the bulk may be described by a charge distribution associated with the dislocation core that, in accordance with theory of screened charges, perturbs the distribution of mobile charge in the material [16]. In particular, the presence of a negative electrostatic potential induces a cloud of positive charges on the GB core, as shown in Fig. 3. While our measurements are consistent with GB charging and the conventional picture [7] that the role of Ca doping is to reduce the height and

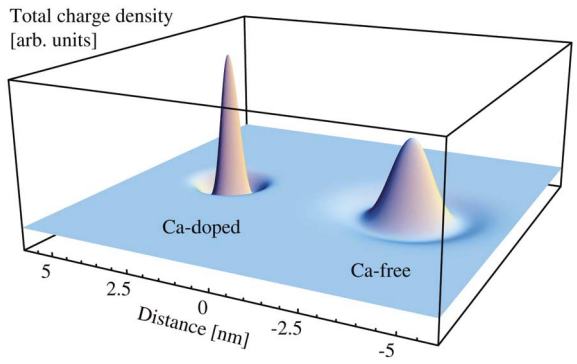

FIG. 3 (color). Representation of the total charge distribution around the dislocation cores. Total charge density for 4° [001] tilt boundary in Ca-doped (left) and undoped (right) YBCO obtained from Poisson's equation applied to the Gaussian potentials shown in Fig. 2. For clarity, the plots are shown as density of *electrons* per unit cell, i.e., the core center corresponds to negative charge.

width of the GB potential, we emphasize that we measure a *negative* potential, in contradiction with the speculation of a *positive* potential leading to hole depletion. We consider in detail, however, the consequence of a negative GB potential and find that, in the framework of electronic band structure, it may lead to an insulating state and depletion of *mobile* charge carriers, consistent with previous experimental findings [7–9].

Electron-electron interaction plays an important role in forming the electronic band structure of YBCO. For $YBa_2Cu_3O_6$ the highest d band in the CuO_2 planes (half occupied) is split into a lower and an upper Hubbard band due to on-site electron-electron repulsion [17], forming a Mott-Hubbard insulator. Oxygen addition results in hole doping of the lower Hubbard band (LHB). Approximating the Hubbard bands as a 2D system, the density of states is constant, and we estimate in this case the Fermi level $E_F = 1.16$ eV and width of the LHB $E_{\mathrm{LHB}} = 1.63$ eV for the Ca-free YBCO [18]. In Fig. 4(a) we compare the energy level of our measured negative potential in the dislocation core with the calculated width of the LHB in the bulk. The electrochemical potential clearly lies far outside the LHB, which has drastic consequences on the local electron states in the core. In Fig. 4(c), the band occupation, which is related to the distribution of mobile charges, is depicted in a continuum (band bending) description. The main effect of the negative potential is to completely fill the band with holes such that the core region is depleted of mobile charge carriers. In the Ca-doped case, we assume the LHB is unchanged and the only difference is the electron and hole occupation where the Fermi level becomes $E_F = 0.997$ eV due to hole doping by Ca [18]. As shown in Fig. 4(b), we measure a potential that is consistent with an emptied LHB or with residual conductivity inverted to n type. In either case, within this framework there is a significant depletion of mobile charge carriers due to screening effects, although less dramatic in the Ca-doped sample.

We assumed above that the measured projected potential is uniform in the beam direction of the microscope, i.e., uniform in the c-axis direction of the sample. If the projected potential varied significantly on the nanometer scale in the c-axis direction, it is possible that the effect of the negative potential described above is either overestimated or underestimated depending on how the potential actually varied along the c-axis direction. Given the in-plane size of the potential, it seems unlikely that the potential would vary enough, and on such a fine enough scale, as to significantly affect the qualitative description we have given. More seriously, however, it is important to point out that application of a continuous band bending scenario is limited in a Mott-Hubbard system where (i) the average electron-electron distance is of the same

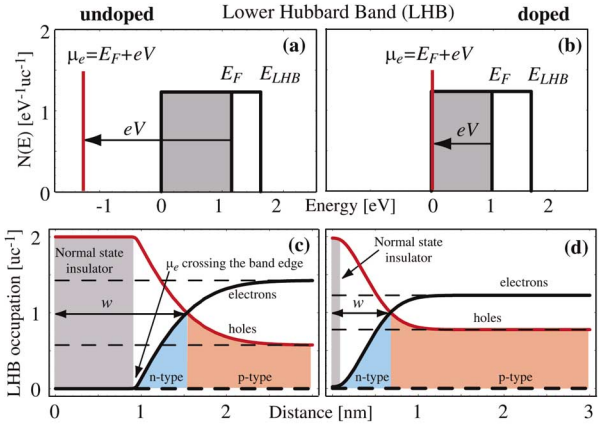

FIG. 4 (color). Density of states and LHB occupation. Top panels show the effect of a negative electrostatic potential V on the electrochemical potential μ_e at the center of dislocation cores for (a) Ca-free and (b) Ca-doped YBCO. The occupation of the LHB is, for electrons, $n = N(E)E_F$, where E_F is the Fermi level measured with respect to the lower band edge, while for holes $p = N(E)(E_{\mathrm{LHB}} - E_F)$, where E_{LHB} is the width of the LHB. For a 2D system, the density of states $N(E) = 8\pi m_e/(ch)^2 = 7.13 \times 10^{27}\ \mathrm{m^{-3}\,eV^{-1}}$ is constant. $YBa_2Cu_3O_7$ corresponds to 0.287 holes per CuO_2 plane ($p = 3.33 \times 10^{27}\ \mathrm{m^{-3}}$) using bond-valence-sum analysis, and the density of electrons therefore is $(1 - 0.287) = 0.713$ per CuO_2 plane ($n = 8.27 \times 10^{27}\ \mathrm{m^{-3}}$). This gives $E_F = 1.16$ eV and $E_{\mathrm{LHB}} = 1.63$ eV for the Ca-free YBCO. In the Ca-doped case, 20% Ca doping brings an additional 0.2 holes per unit cell to the system, hence $p = 0.387$ holes and $n = 0.613$ electrons per CuO_2 plane, and $E_F = 0.997$ eV. In both samples, the measured potential lies at, or well below, the lower band edge. Bottom panels show the spatial variation (from the center of the dislocation cores) of electron and hole occupation per unit cell of the lower Hubbard band for (c) undoped and (d) doped samples. The chemical potential crossing the lower band edge leads to an insulating state. The width w corresponds to the core region where the carrier type is inverted and represents the spatial extent we presume acts as a barrier to flow of supercurrent.

order as the electronic screening length and (ii) the band structure is strongly influenced by electron-electron correlation. Therefore, the numbers calculated above should be taken to point out *qualitative* aspects of the measured negative potentials. Nevertheless, independent of details in the calculation, the negative GB potential is large compared to the width of the bulk LHB, and must therefore have a dramatic effect on the local electron states and their occupation. In the more general "nonlinear" picture of highly correlated electrons with a variety of different competing electronic phases, the negative GB potential could just reflect an insulating phase in the strongly overdoped region not present in the bulk phase diagram. The spatial extent of this insulating phase seems to be strongly reduced by Ca doping.

Independent of the microscopic interpretation, which requires more theoretical and experimental work, our results provide clues to the understanding of the suppressed GB critical current density. It is likely that the core regions act as transport barriers for YBCO in the superconducting state with a barrier radius w and distance L between cores. The average current density across the GB, therefore, is diminished by a factor α, where $J_{GB} = \alpha J_{bulk}$, and represents the fractional area of the GB that can support transport [19], i.e., $\alpha = (L - 2w)/L$, where L is the distance between cores (measured $L =$ 5.3 nm) and w is the "barrier" radius of cores. Taking w to be the radius for carrier inversion (0.7 and 1.5 nm for doped and undoped, as in Fig. 4) we obtain an estimate for Ca-YBCO, $J_{GB}/J_{bulk} = 0.74$, while $J_{GB}/J_{bulk} = 0.43$ for undoped YBCO. This is an improvement in J_c by 31% for Ca-doped samples, and is in very good agreement with MO measurements of these same samples showing 35% increased J_c [14]. This simple model suggests the major contribution to the current density enhancement of Ca-doped YBCO is the reduced core size for these low-angle GBs. It is possible that substitution of Y^{3+} by Ca^{2+} at the dislocation core helps to reduce the lattice strain and core size at the GB [20], which is, moreover, consistent with Ca segregation at GB dislocations in YBCO as observed by Song *et al.* [21].

For high-angle GBs, where the dislocation cores significantly overlap, the simple model described above no longer applies [19], and, as suggested by our data, the reduction of the potential barrier itself, together with a reduction of the barrier width by Ca doping, supports an increased tunneling current. Both of these effects are particularly crucial in terms of superconducting properties since the coherence length of the superconducting condensate, which is roughly 1.4 nm in the *ab* plane at low temperature [22], is close to the GB widths we have measured. Consequently, the decrease in the height and the width of the GB potential appears to be the underlying mechanism for improved GB properties by Ca doping. The evidence for depletion of available carriers at the dislocation cores explains the suppression of superconducting critical currents across grain boundaries as observed for more than a decade in all transport measurements.

The work conducted at Brookhaven was supported by the Division of Materials Sciences, Office of Basic Energy Science, U.S. Department of Energy. The work conducted at Göttingen was partially supported by the DFG (Deutsche Forschungs Gemeinschaft). We gratefully acknowledge helpful discussions with J. Mannhart, D. O. Welch, and M. Suenaga.

*Corresponding author.
Email address: schofield@bnl.gov

[1] E. Dagotto, *Nanoscale Phase Separation and Colossal Magnetoresistance*, Springer Series in Solid State Sciences Vol. 136 (Springer-Verlag, Berlin, 2003).
[2] S. Maekawa and T. Tohyama, Rep. Prog. Phys. **64**, 383 (2001).
[3] K. M. Lang *et al.*, Nature (London) **415**, 412 (2002).
[4] H. A. Mook, D. Pengcheng, and F. Dogan, Phys. Rev. Lett. **88**, 097004 (2002).
[5] J. Zaanen and O. Gunnarsson, Phys. Rev. B **40**, 7391 (1989).
[6] J. Zaanen, Nature (London) **415**, 379 (2002).
[7] H. Hilgenkamp and J. Mannhart, Rev. Mod. Phys. **74**, 485 (2002).
[8] N. D. Browning *et al.*, Physica (Amsterdam) **212C**, 185 (1993).
[9] S. E. Babcock *et al.*, Physica (Amsterdam) **227C**, 183 (1994).
[10] A. Gurevich and E. A. Pashitskii, Phys. Rev. B **57**, 13 878 (1998).
[11] Y. Aharonov and D. Bohm, Phys. Rev. **115**, 485 (1959).
[12] Ch. Jooss, J. Albrecht, H. Kuhn, S. Leonhardt, and H. Kronmüller, Rep. Prog. Phys. **65**, 651 (2002).
[13] Ch. Jooss and J. Albrecht, Z. Metallkd. **93**, 1065 (2002).
[14] K. Guth, H. U. Krebs, H. C. F. Freyhardt, and Ch. Jooss, Phys. Rev. B **64**, 140508(R) (2001).
[15] M. A. Schofield, L. Wu, and Y. Zhu, Phys. Rev. B **67**, 224512 (2003).
[16] J. N. Chazalviel, *Coulomb Screening by Mobile Charges* (Birkhauser, Boston, 1998).
[17] W. E. Pickett, Rev. Mod. Phys. **61**, 433 (1989).
[18] Here we make estimates of the carrier density and electronic bandwidth within a simplified model only to visualize the effect of a negative potential. The values obtained in this first-order approximation are similar to values obtained by other treatments, for example, as in Ref. [10].
[19] D. Agassi, D. K. Christen, and S. J. Pennycook, Appl. Phys. Lett. **81**, 2803 (2002).
[20] H. Su, Ph.D. thesis, SUNY Stony Brook, 2002.
[21] X. Song, J. Buban, N. Browning, and D. C. Larbalestier, in Proceedings of the MRS'02 Fall Meeting, Conference of the Materials Research Society, Boston, MA, 2002 (unpublished).
[22] D. Varshney, R. K. Singh, and S. Shah, J. Supercond. **9**, 629 (1996).